Journal of Data Acquisition and Processing
ISSN: 1004-9037
https://sjcjycl.cn/
DOI: 10.5281/zenodo.776656

COMPRESSED CONTOUR CUMULATIVE GLCM TEXTURE ANALYSIS MODEL BASED CNN FOR PALMPRINT RECOGNITION SYSTEM

Abirami B[1], Krishnaveni K[2]
[1]Research Scholar, [1]Sri S.Ramasamy Naidu Memorial College, (Affiliated to Madurai Kamaraj University), Sattur, Tamilnadu, India. [1]abirami@vhnsnc.edu.in
[2]Associate Professor,
[2]Sri S.Ramasamy Naidu Memorial College, (Affiliated to Madurai Kamaraj University), Sattur, Tamilnadu, India.
[2]kkrishnaveni@srnmcollege.ac.in

Abstract
In this research paper, Compressed Contour Cumulative GLCM Texture Analysis Model based CNN for Palmprint Recognition (3CGLCM-CNN_{Net}) System is proposed to make up the higher level security assurance in the biometric technology. It can be imparted by second-order statistics using a Cumulative Gray-Scale Level Co-occurrence Matrix (CGLCM) feature extraction approach and Convolution Neural Network (CNN_{Net}) classification approach. To enact this, Two Dimensional-Palmprint Region of Interest (2D-PROI) is pre-processed and contour of 2D-PROI image (C_P) is captured using canny edge detection algorithm. Linear Hybrid Conventional Compression Algorithm (LHCC) is applied to constitute the compressed contour 2D-PROI (CC_{PI}) image. In this LHCC algorithm, conventional Discrete Wavelet Transform (DWT) and Principal Component Analysis (PCA) compression algorithms is composited in a linear manner on C_P. Ideal second-order statistical texture features of CC_{PI} are clipped using CGLCM approach. Ideal features are forwarded into 3CGLCM-CNN_{Net} classification algorithm to match the recognized persons. Research is worked on 2D-PROI data derived from the POLYU database, Hong Kong Polytechnic University, Hong Kong. Our proposed system's benchmark has been evaluated and tabulated with higher acceptance of 99% recognition accuracy compared with other existing approaches in biometric technology.

Keywords: Biometric Technology, Palmprint Biometric Trait**,** Gray-Scale Level Co-occurrence Matrix, Convolution Neural Network, Two Dimensional-Palmprint, Region of Interest, Canny edge detection, District Wavelet Transform, Principal Component analysis, Statistic texture features.

1. INTRODUCTION

With [1] the far reaching of computers and cell phones, authentication process utilizes biometrics with greater attention. Howbeit, biometric technology gives great solutions to the recognition performance, because of changing circumstances and maturing of biometric information, which results in intra-class variability. There are two types [2] of biometric system. They are physiological and behavioral type of biometrics. Physiological biometric involves Finger prints, Face recognition, DNA, Palm print and Iris recognition. Behavioral biometric involves gait and voice.

Amid all biometric traits, the palmprint trait is progressing promptly due to its consistent, feasibility at low economical and discriminating ability [3], [4]. Palmprint Recognition System (PRS) is an automatic structural system for ensuring the providence of highly accurate productivity and feasibility of biometric technology. Palmprint [5] is the skin patterns of the inner surface of the human hand from the wrist to the base of the fingers, which give steady and particular data adequate for isolating a person from a large population.

Texture based technique [6] of feature extraction used to separate the feature highlights from palmprint images. Palmprint has numerous texture features to separate which is a rich methodology contains the more texture features. Researchers are synthesizing their research on texture feature extraction due to the more suitability of different feature content withdrawal from an individual [7]. Zhang and Shu [8] have exposed that the placement and direction of the palmprint lines are utilized to recognize the palmprint from others. And those palmprint lines are not indistinguishable to each one [9]. Canny edge detection algorithm is the outstanding algorithm for sensing all edges in the entire palmprint image [10].

Data compression techniques are used for consuming the large bandwidth and storage space of an image [11]. The Discrete Cosine Transform (DCT) and Discrete Wavelet Transform (DWT) are most used superior compression algorithms to produce the less quantized vector by focusing the important signal into low frequency component using less computational resources [11]. DCT has few limitations. One of that is easily point-out the false edges at higher compression [11]. DWT is suitable to provide sampling information of image at different location and frequency [25]. Higher **c**ompression can be easily achieved using DWT[11]. DWT can be composed of wavelet functions with the viability of multi-resolution analysis that takes apart the finer details of signal in an image [12]. Aree and Jamal [13] projected a mixture transform scheme for medical image compression using the DWT and DCT [14]. Principal Component Analysis (PCA) algorithm is another familiar compression algorithm for cutting the image dimensions into low dimension due to its capability of taking-off the continual unnecessary information [15]**.** Composite of two or more compression techniques provides more benefits than the use of one compression technique [11]. This type of composite of two or moreapproaches is referred as “Hybrid Approaches” [11]. [17] After such a reduction of image dimension, statistical feature values are extrapolated by the Gray-Level Co-occurrence Matrix (GLCM) approach [18]. [19] Predominantly Texture-based feature extraction approaches are Gray Level Co-occurrence Matrix [20], [21], Gabor filters [22], Haar filters [23], Daubechies filters [24]-[27] etc. Saban and Byram [28] used the Gray-Level Co-occurrence Matrix, Local Binary Pattern, LBGLCM, GLRLM, and SFTA algorithms to extract the various texture features and compared the results of these algorithms for attaining the effective algorithm for classification [29]**.** [17] Authors in [18] used GLCM technique to clutch the textural informationin the gray-level spatial dependences present in the image [30, 31]. From the attained GLCM, several Texture-based statistical parameters could be derived using different formulas and used CNN for achieving the 97% accuracy of classification [21].

[32] The System could become an intelligent device using machine learning techniques, several techniques are involved such as fuzzy logic, artificial neural network, particle swarm optimization, and although deep learning technique gives better result with huge datasets [33]. Subpart of the deep learning technique is convolution neural networks (CNN) used for automated classification at low computation time with higher performance. Alpana Jijja, Dinesh Rai authors [28] proposed GLCM and Discrete Wavelet Transformation (DWT) technique to detect and label the tumor from an image based on the textures and categorizing a tumor or non- tumor category using Convolution Neural Network (CNN) with the recognition accuracy of 91%. Beura et al. [37] planned GLCM, 2D-DWT and two sample t test and F test filter method, with BPNN classifier, and reported 98.0% accuracy for the Mammographic Image Analysis Society (MIAS).

Wherefore, proposed research work is developed for contributing an efficient PRS to biometric technology. It can be consummated by utilizing the innovative 3CGLCM-CNN_{Net} system that has specific feature extraction approach CGLCM to point-out the essential features and CGLCM-CNN_{Net} classifier to identify the correct authenticated person with 99% accuracy of recognition. Proposed research methodology is depicted in the section 2. Section 3 deals the trained CGLCM-CNN_{Net} classifier algorithm.

2. PROPOSED METHODOLOGY

The proposed Compressed Contour Cumulative GLCM Texture Analysis Model based CNN_{Net} (3CGLCM-CNN_{Net}) system for PRS is performed in four levels: 1. Data acquiring level, 2. Pre- processing level, 3. Feature extraction level, and 4. Classification or Matching level [1]. The recognition and verification processes of 3CGLCM-CNN_{Net} System are depicted in Fig.1, and Fig.2.

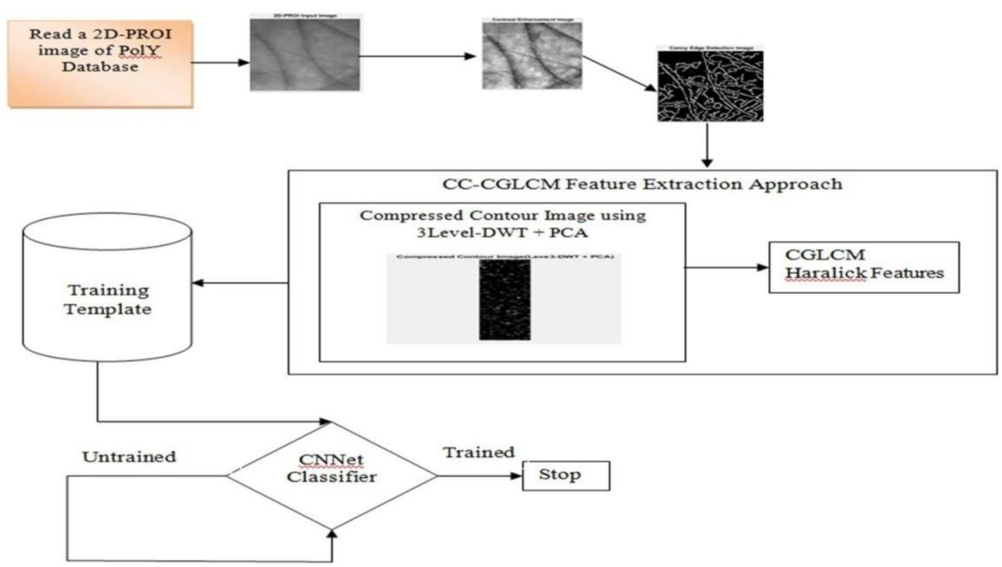

Fig.1. Flow Diagram of 3CGLCM-CNN_{Net} System Recognition Process

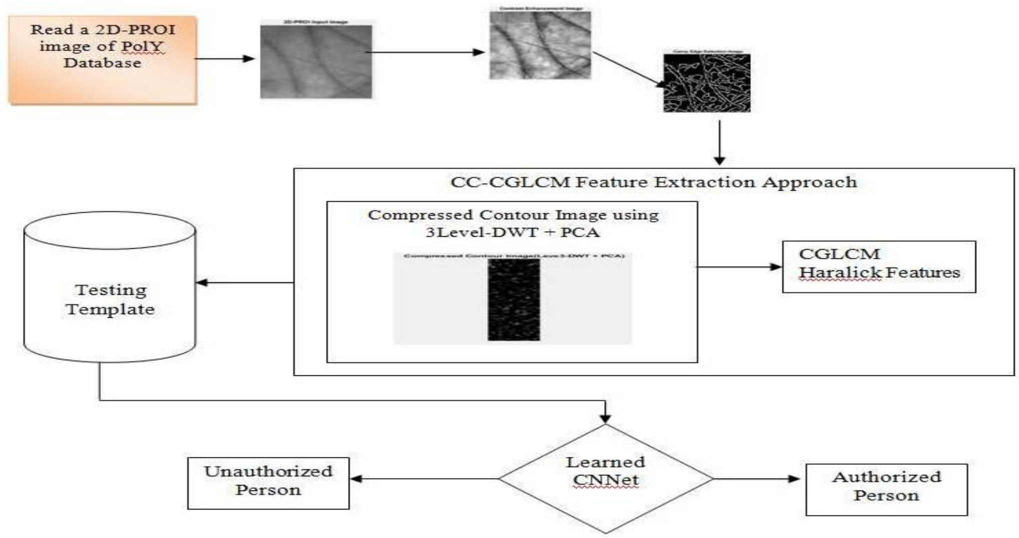

Fig.2. Flow Diagram of 3CGLCM-CNN$_{Net}$ System Verification Process

2.1 Data Acquiring Level

In this research, dataset is taken from POLYU Multi spectral 2D-ROI palmprint database. That contains 8000 normalized 2D-PROI images in .bmp files which are extracted from 400 volunteers' both hands palms and assembled in two different sections. Each section consists of 10 images of right or left hand palm. Fig.3 shows the few POLYU Multi spectral 2D-ROI palmprint images.

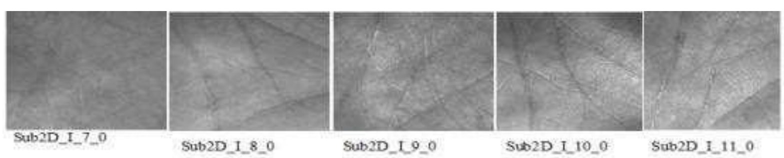

Fig. 3. POLYU 2D-PROI Bitmap Images

2.2 Pre-processing Level

The pre-processing process is needed to exhibit the quality of input image to do further process on it. In this pre-processing, unneeded data are to be got-rid to estimate the correct information of input data. Our research work is started from pre-processing processes that is comprised of conversion of gray-scale image, removal of noise data; enrich the spatial intensity of an input image, tracing the contours of input image. This research work pre-processing images are revealed in Fig 4 (a), (b), and (c).

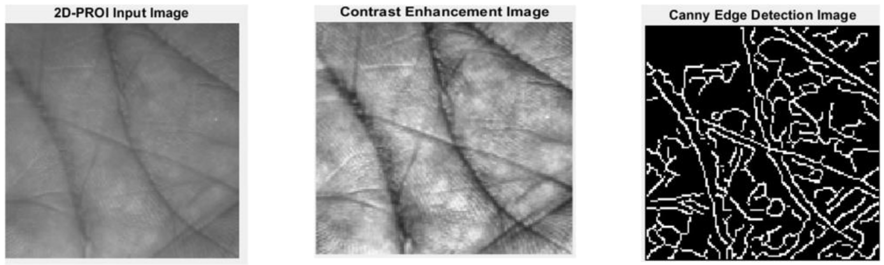

Fig. 4.a.2D-PROI Input Image b. Contrast Enhancement Image of 2D-PROI Image c. Canny Edge Detection of 2D-PROI Image

2.3 Feature Extraction Level

A set of Second-order statistical based texture features of an image can be excerpted by taking advantage of the Compressed Contour Cumulative Gray-Scale Co-occurrence Matrix (CC-CGLCM) move toward in a quirky way. The initial step of executing the CC-CGLCM approach is to produce the Compressed Contour Pre-processing Image (C_P) by crossover the two natural compression algorithms in a linear manner (DWT and PCA). Fig.6 depicts the graphical representation of LHCC algorithm. This proposed LHCC algorithm is compressed the C_P image of size (128 × 128) into CC_{PI} image of size (64 × 16). This compression makes the calculation rapidly and effectively at the stipulated time with lots of information. After the CC_{PI} created, GLCMs are made from CC_{PI} based on Ɵ (i.e. Ɵ = 0°, 45°, 90°, 135°, 180°, 225°, 270°, and 315°) to know the incarnated high frequency of the pixel [29], which is displayed in Fig.5 and combined all GLCMs to frame a Cumulative GLCM (CGLCM). This approach is proclaimedin section 2.3.1.

Statistical methods are the most important used method to define the Second-order texture on the gray-scale spatial intensity at the each pixel of the entire image. Second-order statistics features are plucked from GLCM that defines the possessiveness between gray-scale pixels of images. Second order methods provide higher discrimination rates than any other methods [18]. In 1973, Haralick et al have invented 14 textural features were derived from GLCM matrices [18]. Second-Order statistics features are extricated using CGLCMs, which are described in section 2.3.2 and 3.3.2. Pick-out of few Haralick's features such as energy, contrast, homogeneity, entropy and correlation of gray level's spatial relationship between pixels in the normalized CGLCM to percept the different dimension of texture information [18].

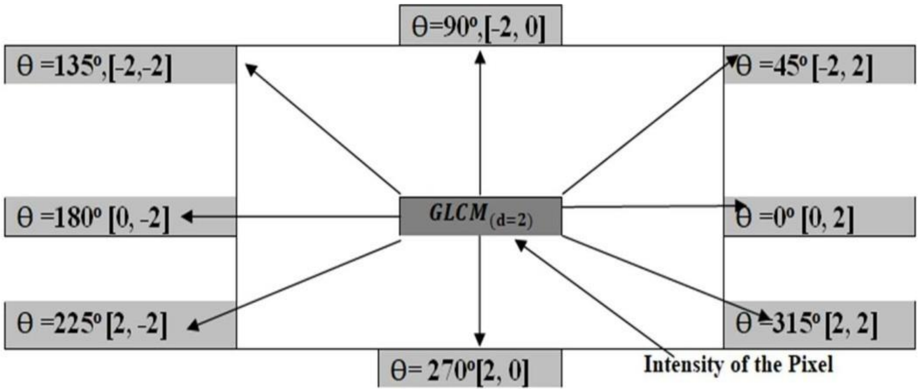

Fig.5. Diagrammatic Representation of GLCM's with various Ɵs

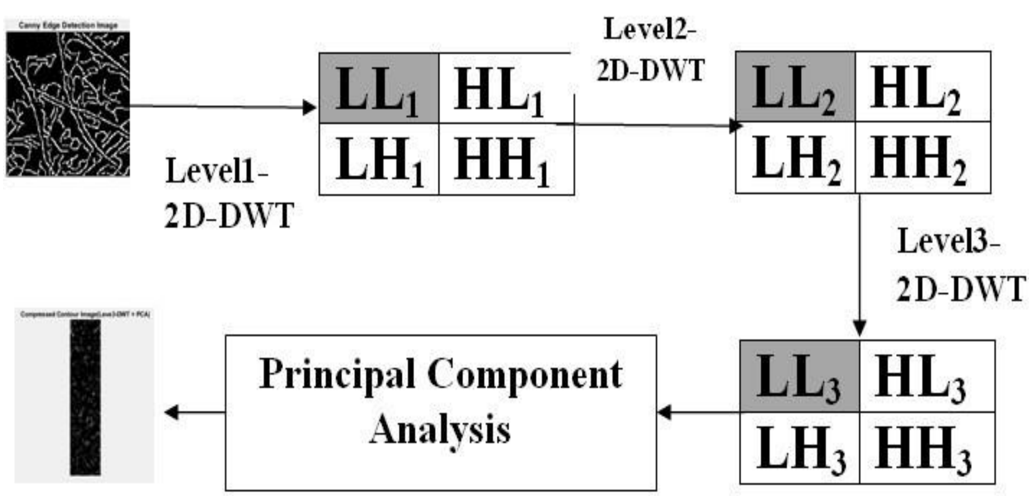

Fig.6. Pictorial Representation of LHCC Algorithm

2.3.1 CC-CGLCM approach is implemented as follows

Step 1: C_P is compressed using LHCC Algorithm, which is described as below:

A, At DWT-Level1, C_P is compressed into 4 sub-band images (i.e. LL_1, HL_1, LH_1, and HH_1).

B, At DWT-Level2, LL_1 of C_P is compressed into another 4 sub-bands (i.e. LL_2, HL_2, LH_2, and HH_2).

C, At DWT-Level3, LL_2 of C_P is compressed into another 4 sub-bands(i.e. LL_3, HL_3, LH_3, and HH_3).

D, Reduced the dimensionality of LL_3 using PCA algorithm. It produced the CC_{PI}, which is delineated in Fig.6.

Step 2: Generate the eight $GLCM_{CC_{PI}}$ with eight different orientations such as $GLCM_{(d=2,\theta=0^0)}$, $GLCM_{CC_{PI}(d=2,\theta=4\ ^0)}$, $GLCM_{CC_{PI}(d=2,\theta=9\ ^0)}$, $GLCM_{CC_{PI}(d=2,\theta=135^0)}$, $GLCM_{CC_{PI}(d=2,\theta=180^0)}$, $GLCM_{CC_{PI}(d=2,\theta=275^0)}$, $GLCM_{CC_{PI}(d=2,\theta=225^0)}$, $GLCM_{CC_{PI}(d=2,\theta=315^0)}$ matrices, which is displayed in Fig.9.

Step 3: Eight different directions GLCM matrices are cumulated to form a $CGLCM_{\mathrm{CC_{PI}}}$ using (1).

$$CGLCM_{\mathrm{CC_{PI}}} = \sum\left(\sum_{i=1}^{8} GLCM_{\mathrm{CC_{PI}}_{(i)}} + \sum_{i=1}^{8} GLCM_{\mathrm{CC_{PI}}_{(i)}}{}^{T}\right) \tag{1}$$

Step 4: Haralick's features are extracted from $CGLCM_{\mathrm{CC_{PI}}}$ of size (8× 8) using (11), (12), (13), (14), and (15).

2.3.2 Extraction of Haralicks' Features is described as follows

G is the number of gray levels used in the $CGLCM_{\mathrm{CC_{PI}}}$. $NCGLCM_{\mathrm{CC_{PI}}}$ is computed from $CGLCM_{\mathrm{CC_{PI}}}$ matrix using (2). μ is the mean value of $NCGLCM_{\mathrm{CC_{PI}}}$. μ_x, μ_y, σ_x and σ_y are the means and standard deviations of $NCGLCM_{\mathrm{CC_{PI}}^{x}}$ and $NCGLCM_{\mathrm{CC_{PI}}^{y}}$ using (7), (8), (9), and (10). $NCGLCM_{\mathrm{CC_{PI}}^{x}}(i)$ and $NCGLCM_{\mathrm{CC_{PI}}^{x}}(j)$ is the i^{th} and j^{th} entry in the normalized $CGLCM_{\mathrm{CC_{PI}}}$ matrix using (5) and (6).

$$NCGLCM_{\mathrm{CC_{PI}}} = \frac{\sum_{i=1}^{G}\sum_{j=1}^{G} CGLCM_{\mathrm{CC_{PI}}}(i,j)}{\sum\sum_{i=1}^{G}\sum_{j=1}^{G} CGLCM_{\mathrm{CC_{PI}}}(i,j)} \tag{2}$$

$$S = \sum_{i=0}^{G-1} i \sum_{j=0}^{G-1} NCGLCM_{\mathrm{CC_{PI}}}(i,j) \tag{3}$$

$$NCGLCM_{\mathrm{CC_{PI}}}(i,j) = \frac{\sum_{i=0}^{G-1} i \sum_{j=0}^{G-1} NCGLCM_{\mathrm{CC_{PI}}}(i,j)}{S} \tag{4}$$

$$NCGLCM_{\mathrm{CC_{PI}}^{x}}(i) = \sum_{j=0}^{G-1} NCGLCM_{\mathrm{CC_{PI}}}(i,j) \tag{5}$$

$$NCGLCM_{\mathrm{CC_{PI}}^{y}}(j) = \sum_{i=0}^{G-1} NCGLCM_{\mathrm{CC_{PI}}}(i,j) \tag{6}$$

$$\mu_x = \sum_{i=0}^{G-1} i \times NCGLCM_{\mathrm{CC_{PI}}^{x}}(i) \tag{7}$$

$$\mu_y = \sum_{i=0}^{G-1} j \times NCGLCM_{\mathrm{CC_{PI}}^{y}}(j) \tag{8}$$

$$\sigma_x = \sqrt{\sum_{i=1}^{G}\sum_{j=1}^{G} (i-\mu_X)^2 \times NCGLCM_{\mathrm{CC_{PI}}}(i,j)} \tag{9}$$

$$\sigma_y = \sqrt{\sum_{i=1}^{G}\sum_{j=1}^{G} (j-\mu_y)^2 \times NCGLCM_{\mathrm{CC_{PI}}}(i,j)} \tag{10}$$

The following features are fetched:

1. **Contrast**

The difference between the dark and light areas between a pixel and its neighborhood in $NCGLCM_{\mathrm{CC\,PI}}$ of an image is calculated.

$$\text{Contrast} = \sum_{i=1}^{G}\sum_{j=1}^{G}(i-j)^2 \times NCGLCM_{\mathrm{CC\,PI}}(i,j) \tag{11}$$

2. **Correlation**

It is defined as the connection of a pixel is to its neighborhood pixels.

$$\text{Correlation} = \sum_{i=1}^{G-1}\sum_{j=1}^{G-1}\frac{(\mathrm{i}-\mu_{\mathrm{x}})\times\left(\mathrm{j}-\mu_{\mathrm{y}}\right)\times NCGLCM_{\mathrm{CC\,PI}}(\mathrm{i,j})}{\sigma_x \times \sigma_y} \tag{12}$$

3. **Energy**

It is an amount of squared components in $NCGLCM_{\mathrm{CC\,PI}}$.

$$\text{Energy} = \sum_{i=1}^{G}\sum_{j=1}^{G} NCGLCM_{\mathrm{CC\,PI}}(i,j)^2 \tag{13}$$

4. **Homogeneity**

It gives a thought regarding the closeness of components in $NCGLCM_{\mathrm{CC\,PI}}$ to its corner to corner component.

$$\text{Homogeneity} = \sum_{i=1}^{G}\sum_{j=1}^{G}\frac{NCGLCM_{\mathrm{CC\,PI}}(i,j)}{1+(i-j)} \tag{14}$$

5. **Entropy**

Image entropy is a quantity; depict the how much data should be coded by a compression algorithm.

$$\text{Entropy} = -\sum_{i=0}^{G-1}\sum_{j=0}^{G-1} NCGLCM_{\mathrm{CC\,PI}}(i,j) \times \log\left(NCGLCM_{\mathrm{CC\,PI}}(\mathrm{i,j})\right) \tag{15}$$

In this way, the five Haralick's element values are made out and put away as the training and testing templates utilizing CC-CGLCM approach.

3. CLASSIFICATION OR MATCHING LEVEL

3CGLCM-CNN$_{\mathrm{Net}}$ classifier is built using Matlab Deep Learning Toolbox in the Matlab R2021a software. Proposed 3CGLCM-CNN$_{\mathrm{Net}}$ classifier is constructed using peculiar parameters. That is clearly given in Table.1. All 3CGLCM-CNN$_{\mathrm{Net}}$ peculiar parameters substitute in the array of layers and used the trainingOptions() method to construct the 3CGLCM-CNN$_{\mathrm{Net}}$. After set the 3CGLCM-CNN$_{\mathrm{Net}}$, training process of 3CGLCM-CNN$_{\mathrm{Net}}$ is processed using trainNetwork() function. Trained 3CGLCM-CNN$_{\mathrm{Net}}$ is found. And this assessment is based on the percentage value of the accuracy present in the training progress chart which is exemplified in Fig.11.

In the implementation of 3CGLCM-CNN_{Net} classifier, training progress chart is generated with the classification percentage of accuracy and loss at every epoch cycle. Based on the obtained accuracy and loss percentage value, the trainingprocess of the 3CGLCM-CNN_{Net} is to be stopped. Fig.11. reveals the 100% of accuracy and 0% of loss in the 3CGLCM-CNN_{Net} System recognition process met at the 30^{th} epoch. Trained 3CGLCM-CNN_{Net} classifier is used at the testing phase.

4. EXPERIMENTAL ANALYSIS

This research is appropriated 400 2D-PROI images of 20 workers in POLYU dataset, on that 80% of training images and 20% of testing image are conveyed for the palmprint identification process. In the testing stage, at first, 100 images tests are made and further expanded in strides of 100 for each testing. Fundamentally, training and testing templates is created utilizing CC-CGLCM feature extraction approach. In this proposed CC-GLCM feature extraction, C_P image dimension of size (128 × 128) is reduced and generated the CC_{PI} image of size (64 × 16) utilizing LHCC algorithm that bears less essential feature extraction values to compose the computation quirky at low recognition time.

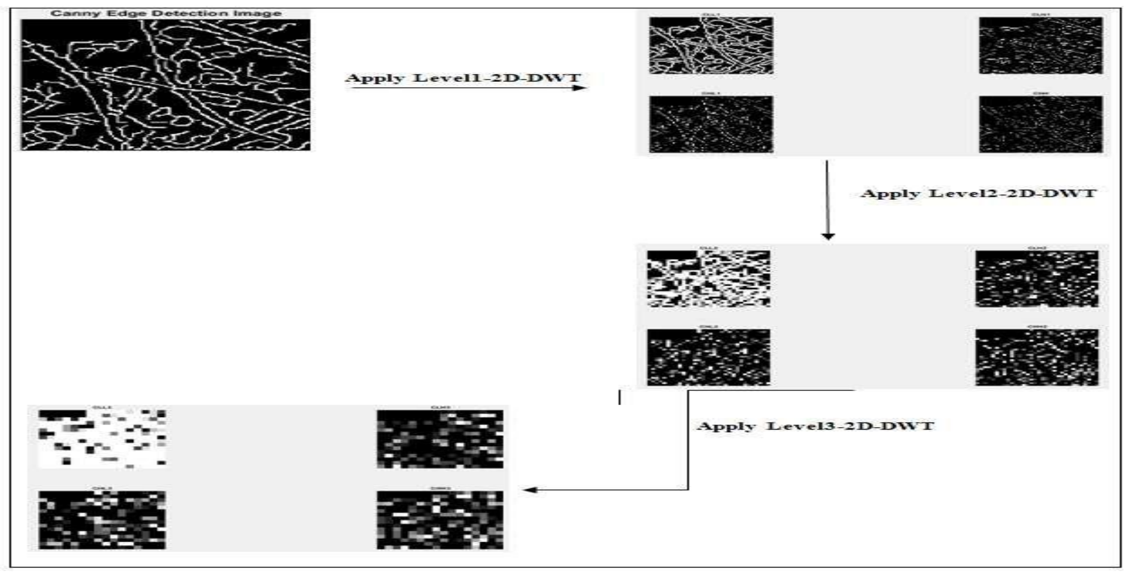

Fig.7. Resultant of DWT-Level3 Algorithm of C_P

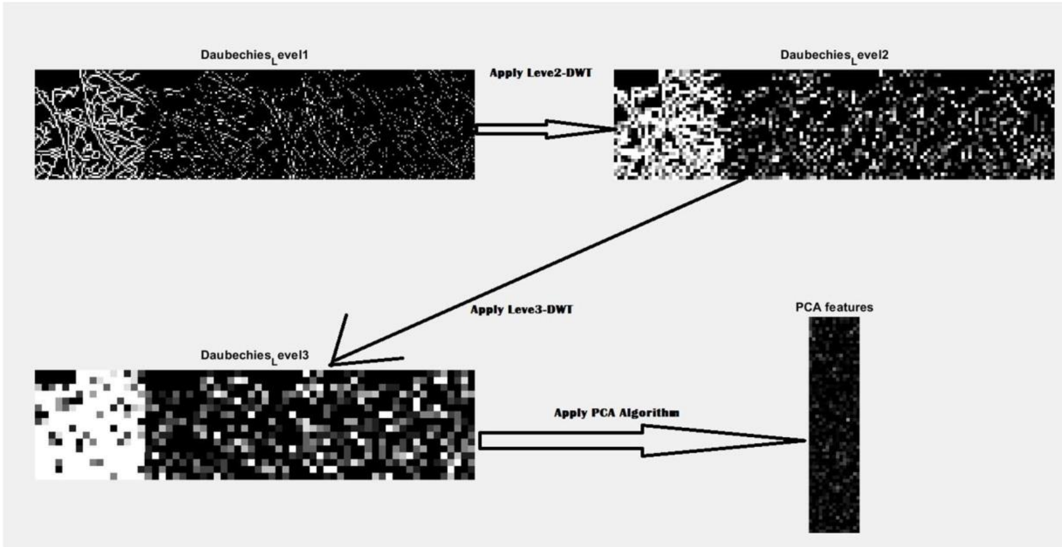

Fig.8. Formation of CC$_{PI}$ Using LHCC Algorithm

Thisprocess is obviously illustrates in Fig. 8. LHCC algorithm is utilized the DWT-Level3, at each level a detailed (D) and an approximated (A) images are derived, on that detailed image of every levelis passed in a linear way to the next level of DWT process for deriving the fine compressed detailed image which are layout in Fig.7.Obtained CC$_{PI}$ image is used for extracting the second-order statistic texture features to make the training and testing templates.

For extracting Haralick's feature, eight Gray-Level Co-occurance Matrices are formed with different orientation from CC$_{PI}$. That is depicted in Fig.9.

$$GLCM_{(d=2,\theta=0^0)} = \begin{bmatrix} 598 & 82 & 22 & 2 & 1 & 0 & 0 & 0 \\ 88 & 15 & 1 & 0 & 0 & 0 & 0 & 0 \\ 13 & 4 & 0 & 0 & 0 & 0 & 0 & 0 \\ 4 & 1 & 0 & 0 & 0 & 0 & 0 & 0 \\ 1 & 0 & 0 & 0 & 0 & 0 & 0 & 0 \\ 0 & 0 & 0 & 0 & 0 & 0 & 0 & 0 \\ 0 & 0 & 0 & 0 & 0 & 0 & 0 & 0 \\ 0 & 0 & 0 & 0 & 0 & 0 & 0 & 0 \end{bmatrix}$$

$$GLCM_{(d=2,\theta=45^0)} = \begin{bmatrix} 581 & 86 & 17 & 2 & 0 & 0 & 0 & 0 \\ 88 & 4 & 5 & 0 & 1 & 0 & 0 & 0 \\ 13 & 3 & 0 & 0 & 0 & 0 & 0 & 0 \\ 3 & 2 & 0 & 0 & 0 & 0 & 0 & 0 \\ 1 & 0 & 0 & 0 & 0 & 0 & 0 & 0 \\ 0 & 0 & 0 & 0 & 0 & 0 & 0 & 0 \\ 0 & 0 & 0 & 0 & 0 & 0 & 0 & 0 \\ 0 & 0 & 0 & 0 & 0 & 0 & 0 & 0 \end{bmatrix}$$

$$GLCM_{(d=2,\theta=90^0)} = \begin{bmatrix} 673 & 89 & 21 & 4 & 1 & 0 & 0 & 0 \\ 95 & 18 & 1 & 0 & 0 & 0 & 0 & 0 \\ 18 & 3 & 0 & 1 & 0 & 0 & 0 & 0 \\ 3 & 2 & 0 & 0 & 0 & 0 & 0 & 0 \\ 1 & 0 & 0 & 0 & 0 & 0 & 0 & 0 \\ 0 & 0 & 0 & 0 & 0 & 0 & 0 & 0 \\ 0 & 0 & 0 & 0 & 0 & 0 & 0 & 0 \\ 0 & 0 & 0 & 0 & 0 & 0 & 0 & 0 \end{bmatrix}$$

$$GLCM_{(d=2,\theta=135^0)} = \begin{bmatrix} 581 & 83 & 13 & 5 & 1 & 0 & 0 & 0 \\ 84 & 12 & 2 & 0 & 0 & 0 & 0 & 0 \\ 19 & 1 & 2 & 0 & 0 & 0 & 0 & 0 \\ 2 & 0 & 0 & 0 & 0 & 0 & 0 & 0 \\ 1 & 0 & 0 & 0 & 0 & 0 & 0 & 0 \\ 0 & 0 & 0 & 0 & 0 & 0 & 0 & 0 \\ 0 & 0 & 0 & 0 & 0 & 0 & 0 & 0 \\ 0 & 0 & 0 & 0 & 0 & 0 & 0 & 0 \end{bmatrix}$$

$$GLCM_{(d=2,\theta=270^0)} = \begin{bmatrix} 673 & 95 & 18 & 3 & 1 & 0 & 0 & 0 \\ 89 & 18 & 3 & 2 & 0 & 0 & 0 & 0 \\ 21 & 1 & 0 & 0 & 0 & 0 & 0 & 0 \\ 4 & 0 & 1 & 0 & 0 & 0 & 0 & 0 \\ 1 & 0 & 0 & 0 & 0 & 0 & 0 & 0 \\ 0 & 0 & 0 & 0 & 0 & 0 & 0 & 0 \\ 0 & 0 & 0 & 0 & 0 & 0 & 0 & 0 \\ 0 & 0 & 0 & 0 & 0 & 0 & 0 & 0 \end{bmatrix}$$

$$GLCM_{(d=2,\theta=225^0)} = \begin{bmatrix} 581 & 88 & 13 & 3 & 1 & 0 & 0 & 0 \\ 86 & 4 & 3 & 2 & 0 & 0 & 0 & 0 \\ 17 & 5 & 0 & 0 & 0 & 0 & 0 & 0 \\ 2 & 0 & 0 & 0 & 0 & 0 & 0 & 0 \\ 0 & 1 & 0 & 0 & 0 & 0 & 0 & 0 \\ 0 & 0 & 0 & 0 & 0 & 0 & 0 & 0 \\ 0 & 0 & 0 & 0 & 0 & 0 & 0 & 0 \\ 0 & 0 & 0 & 0 & 0 & 0 & 0 & 0 \end{bmatrix}$$

$$GLCM_{(d=2,\theta=180^0)} = \begin{bmatrix} 598 & 88 & 13 & 4 & 1 & 0 & 0 & 0 \\ 82 & 15 & 4 & 1 & 0 & 0 & 0 & 0 \\ 22 & 1 & 0 & 0 & 0 & 0 & 0 & 0 \\ 2 & 0 & 0 & 0 & 0 & 0 & 0 & 0 \\ 1 & 0 & 0 & 0 & 0 & 0 & 0 & 0 \\ 0 & 0 & 0 & 0 & 0 & 0 & 0 & 0 \\ 0 & 0 & 0 & 0 & 0 & 0 & 0 & 0 \\ 0 & 0 & 0 & 0 & 0 & 0 & 0 & 0 \end{bmatrix}$$

$$GLCM_{(d=2,\theta=315^0)} = \begin{bmatrix} 581 & 84 & 19 & 2 & 1 & 0 & 0 & 0 \\ 83 & 12 & 1 & 0 & 0 & 0 & 0 & 0 \\ 13 & 2 & 2 & 0 & 0 & 0 & 0 & 0 \\ 5 & 0 & 0 & 0 & 0 & 0 & 0 & 0 \\ 1 & 0 & 0 & 0 & 0 & 0 & 0 & 0 \\ 0 & 0 & 0 & 0 & 0 & 0 & 0 & 0 \\ 0 & 0 & 0 & 0 & 0 & 0 & 0 & 0 \\ 0 & 0 & 0 & 0 & 0 & 0 & 0 & 0 \end{bmatrix}$$

Fig.9. Obtained Eight GLCMs with different Orientation from CCPI

CGLCM is generated using (1) and its resultant value is given below:

$$CGLCM_{\mathrm{CCPI}} = \begin{bmatrix} 9732 & 1390 & 272 & 50 & 14 & 0 & 0 & 0 \\ 1390 & 196 & 40 & 10 & 2 & 0 & 0 & 0 \\ 272 & 40 & 8 & 2 & 0 & 0 & 0 & 0 \\ 50 & 10 & 2 & 0 & 0 & 0 & 0 & 0 \\ 14 & 2 & 0 & 0 & 0 & 0 & 0 & 0 \\ 0 & 0 & 0 & 0 & 0 & 0 & 0 & 0 \\ 0 & 0 & 0 & 0 & 0 & 0 & 0 & 0 \\ 0 & 0 & 0 & 0 & 0 & 0 & 0 & 0 \end{bmatrix}$$

Then, five Haralick's features are extracted from normalized $CGLCM_{\mathrm{CCPI}}$ ($NCGLCM_{\mathrm{CCPI}}$). The resultant value of the $NCGLCM_{\mathrm{CCPI}}$ is shown as below:

$$NCGLCM_{\mathrm{CCPI}} = \begin{bmatrix} 0.7211 & 0.1030 & 0.0202 & 0.0037 & 0.0010 & 0 & 0 & 0 \\ 0.1030 & 0.0145 & 0.0030 & 0.0007 & 0.0001 & 0 & 0 & 0 \\ 0.0202 & 0.0030 & 0.0006 & 0.0001 & 0 & 0 & 0 & 0 \\ 0.0037 & 0.0007 & 0.0001 & 0 & 0 & 0 & 0 & 0 \\ 0.0010 & 0.0001 & 0 & 0 & 0 & 0 & 0 & 0 \\ 0 & 0 & 0 & 0 & 0 & 0 & 0 & 0 \\ 0 & 0 & 0 & 0 & 0 & 0 & 0 & 0 \\ 0 & 0 & 0 & 0 & 0 & 0 & 0 & 0 \end{bmatrix}$$

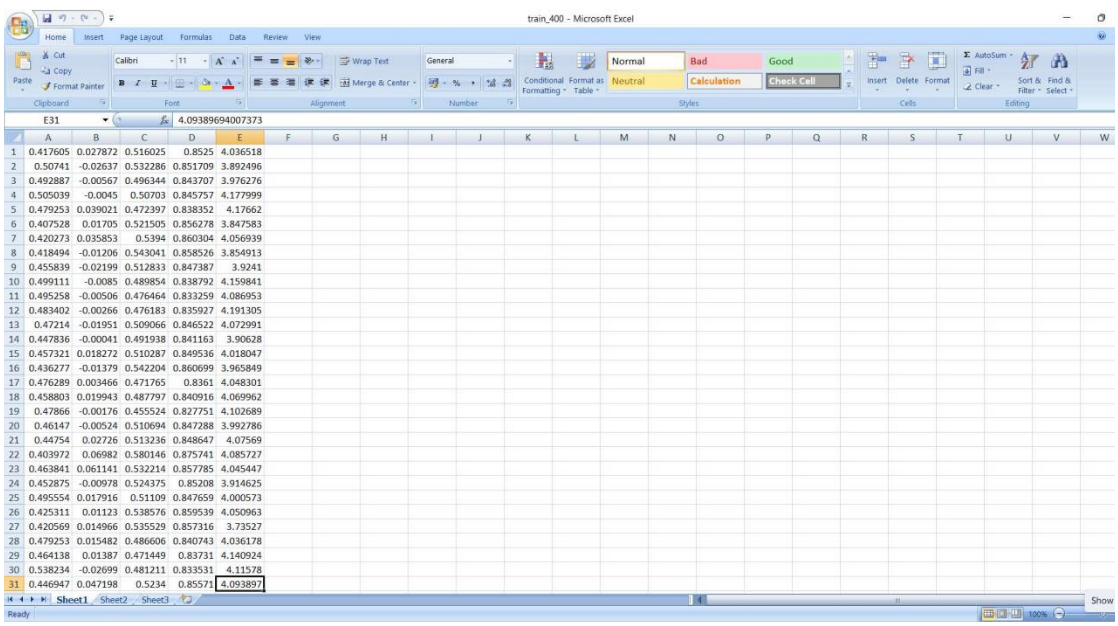

	A	B	C	D	E
1	0.417605	0.027872	0.516025	0.8525	4.036518
2	0.50741	-0.02637	0.532286	0.851709	3.892496
3	0.492887	-0.00567	0.496344	0.843707	3.976276
4	0.505039	-0.0045	0.50703	0.845757	4.177999
5	0.479253	0.039021	0.472397	0.838352	4.17662
6	0.407528	0.01705	0.521505	0.856278	3.847583
7	0.420273	0.035853	0.5394	0.860304	4.056939
8	0.418494	-0.01206	0.543041	0.858526	3.854913
9	0.455839	-0.02199	0.512833	0.847387	3.9241
10	0.499111	-0.0085	0.489854	0.838792	4.159841
11	0.495258	-0.00506	0.476464	0.833259	4.086953
12	0.483402	-0.00266	0.476183	0.835927	4.191305
13	0.47214	-0.01951	0.509066	0.846522	4.072991
14	0.447836	-0.00041	0.491938	0.841163	3.90628
15	0.457321	0.018272	0.510287	0.849536	4.018047
16	0.436277	-0.01379	0.542204	0.860699	3.965849
17	0.476289	0.003466	0.471765	0.8361	4.048301
18	0.458803	0.019943	0.487797	0.840916	4.069962
19	0.47866	-0.00176	0.455524	0.827751	4.102689
20	0.46147	-0.00524	0.510694	0.847288	3.992786
21	0.44754	0.02726	0.513236	0.848647	4.07569
22	0.403972	0.06982	0.580146	0.875741	4.085727
23	0.463841	0.061141	0.532214	0.857785	4.045447
24	0.452875	-0.00978	0.524375	0.85208	3.914625
25	0.495554	0.017916	0.51109	0.847659	4.000573
26	0.425311	0.01123	0.538576	0.859539	4.050963
27	0.420569	0.014966	0.535529	0.857316	3.73527
28	0.479253	0.015482	0.486606	0.840743	4.036178
29	0.464138	0.01387	0.471449	0.83731	4.140924
30	0.538234	-0.02699	0.481211	0.833531	4.11578
31	0.446947	0.047198	0.5234	0.85571	4.093897

Fig.10. Extracted Second-Order Feature values using CC-CGLCM approach

Haralick's features such as Contrast, Homogeneity, Energy, Entropy, and Correlation are created using (11), (12), (13), (14), and (15). For training phase, 400 2D-PROI images' features are extracted; the collected features are shown in Fig.10. Table.1. shows all peculiar parameters used in the 3CGLCM-CNN_{Net} Network frame. The completion of the training process is measured through the accuracy percentage value cited in the training progress chart which is shown in the Fig.11. In this chart, at the level of 30^{th} epoch 100% accuracy and 0% loss is met. This obviously revealed the achievement of high accuracy at low level epoch iteration in 56 seconds.

Table.1 Peculiar Parameters of 3CGLCM-CNN_{Net} for Recognizing the 400 Training Images

Num. Features	Num. Filters	Filter Size	Num. HiddenUnits	Num. Classes	Max Epochs	Mini BatchSize	Learning Rate
1×5×1	12	[3 3]	50	400	100	10	0.001

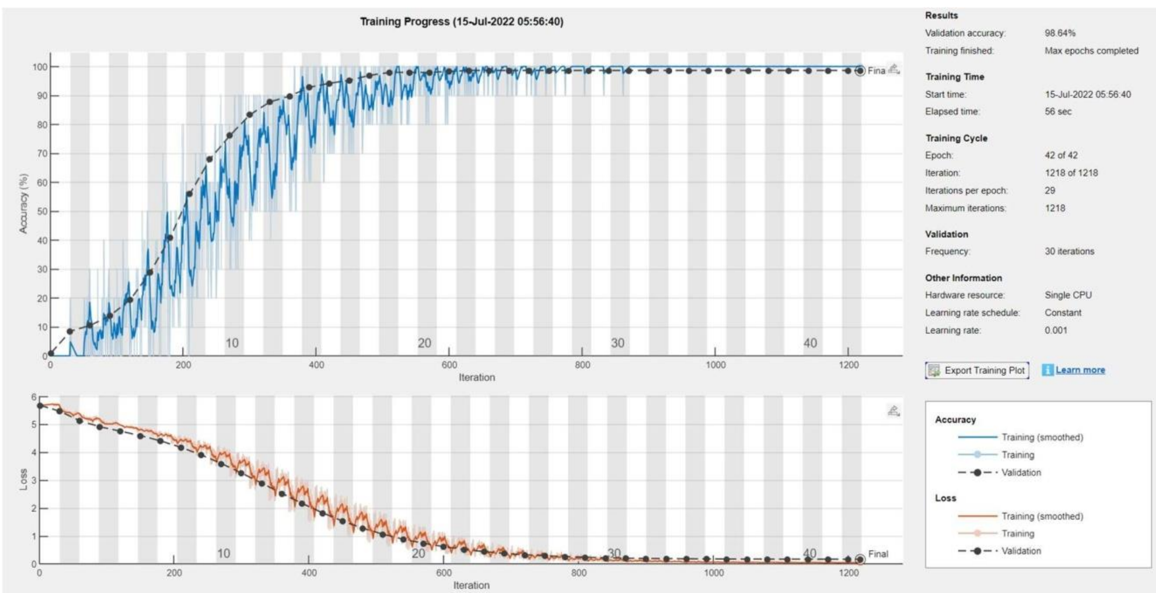

Fig.11. Training Progress chart of 3CGLCM-CNN_{Net} System

The proposed system 3CGLCM-CNN_{Net} classifier benchmark is examined using confusion matrix. Confusion matrix uses the predictive factors; those are computed by checking the Truly Match (TM), Falsie Match (FM), Truly Mismatch (TMM), and Falsie Mismatch (FMM) classes at the identification process of 3CGLCM-CNN_{Net} system. Classification benchmark parameters such as Accuracy, Sensitivity, Fall-Out, Miss Rate, and Specificity are estimated using predictive factors of the confusion matrix by invoking the formulas (17), (18), (19), (20), and(21).

$$\text{Sensitivity} = \frac{TM}{TM+FMM} \tag{17}$$

$$\text{Fall-Out} = \frac{FM}{FMM+TMM} \tag{18}$$

$$\text{Accuracy} = \frac{TM+TMM}{TM+TMM+FM+FMM} \tag{19}$$

$$\text{Miss Rate} = \frac{FMM}{TM+FMM} \tag{20}$$

$$\text{Specificity} = \frac{TMM}{TMM+FM} \tag{21}$$

Obviously Table. 2, and Fig.12 exposes the escalation of TMM at every testing phase with increasing testing templates. 3CGLCM-CNN_{Net} system classification attained the higher accuracy values (0.95, 0.985, 0.9833 and 0.99) at every increasing testing datasets (100, 200, 300, and 400). That's proof the proposed 3CGLCM- CNN_{Net} system is secured the higher security and veracity to identify the authentication person of colossal dataset.

Table.2 Predicted Values of Confusion Matrix Parameters

Number of testing Samples	TP	TN	FP	FN	FNR	FPR	TPR	TNR	CPR
100	80	15	2	3	3.61%	11.76%	96.39%	88.24%	95.00%
200	160	37	2	1	0.62%	5.13%	99.38%	94.87%	98.50%
300	242	53	4	1	0.41%	7.02%	99.59%	92.98%	98.33%
400	321	75	3	1	0.31%	3.85%	99.69%	96.15%	99.00%

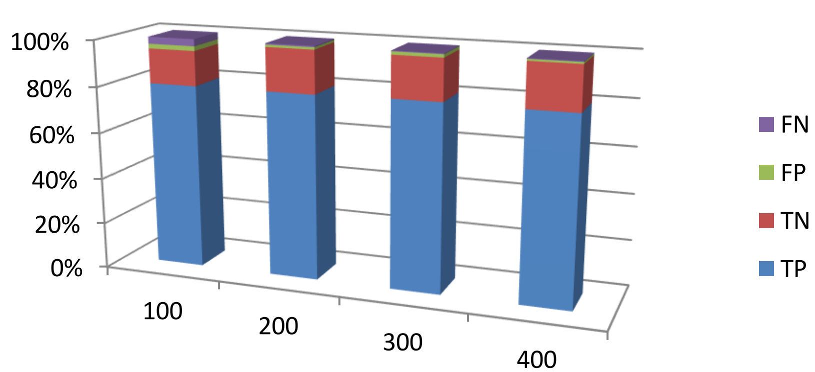

Fig.12. Predicted Values of the Confusion Matrix for Various Ranges of Testing Template

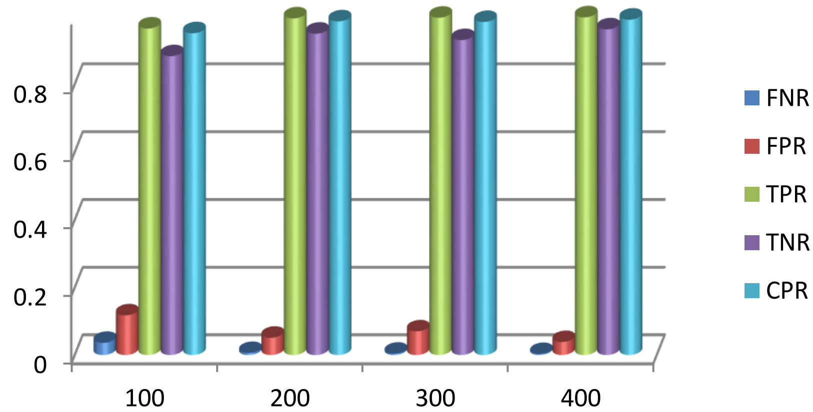

Fig.13. Confusion Matrix Parameter Values for Various Ranges of Testing Template

5. DISCUSSIONS

In this research work, 3CGLCM-CNN$_{Net}$ system gets the best accuracy of 99% in the identification of authenticate persons compare than other existing research paper works. That is obviously revealed on Fig.13. Fig.14 shows the comparative analysis of existing research papers' accuracy along with the proposed system identification accuracy. Fig.12 and Fig.13 acts as proof for considering the 3CGLCM-CNN$_{Net}$ system carry out the mass data correctly and capably. 3CGLCM-CNN$_{Net}$ system will be optimum to pause the unauthorized access of digital data and assets.

Table.3 Comparative Analysis of Existing Recognition Approaches with Proposed Approaches

S.No	Recognition Approaches	Recognition Accuracy Rate	Publication Year
1.	DWT + GLCM feature extraction approach and KNN classifier [34].	95.7%	**2010**
2.	GLCM + Daubechies4 Wavelet + Rotated Wavelet feature extraction approach and Euclidean Distance classifier [35].	85.7%	2011
3.	DMWT + LBP +PCA feature extraction approach and Euclidean Distance classifier [36].	98.4%	2011
4.	GLCM, 2D-DWT and two sample t test and F test filter method, with BPNN classifier.[37]	98.0%	2015
5.	Haar Wavelet Transform + GLCM feature extraction approach, Random Forest classifier [38].	97.39%	2019

6.	Dual Tree Complex Wavelet Transform (DTCWT) and Principal Component Analysis (PCA) feature extraction approach and Mahalanobis distance classifier [39].	98%	2020
7.	GLCM feature extraction approach +DNN classifier [40].	98%	2020
8.	GLCM and Discrete Wavelet Transformation (DWT) feature extraction approach and CNN classifier [41].	91%	2020
9.	DWT + GLCM feature extraction approach, and SVM+RBF classifier [42].	93.62%	2021
10.	Proposed 3CGLCM-CNN_{Net} System	99%	---------

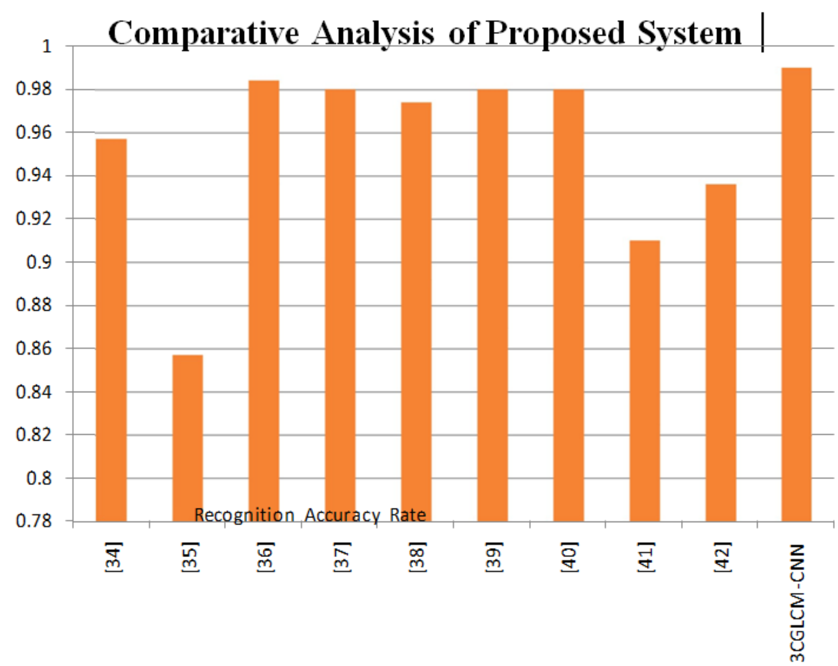

Fig.14. Comparative Chart of Proposed 3CGLCM-CNN_{Net} System

6. CONCLUSION

Proposed 3CGLCM-CNN_{Net} system is fostered to extricate the affluent features using second-order statistics (CGLCM) approach and classify the accurate person authentication using CNN_{Net} from the low dimension input CC_{PI} image using LHCC algorithm. 3CGLCM-CNN_{Net} system research is provoked on 400 POLYU 2D-PROI dataset, on that 80%, 20% is taken for training and testing phase. Analyzing the recognition rate of existing recognition systems with the higher achievement of 99% in the proposed system recognition rate make known that the proposed 3CGLCM-CNN_{Net} system can be considered as one of the securable PRS. In future research, extendable of the feature selection and extraction process will be essential to escalate the recognition accuracy into 100% that only will make a worthy PRS to the biometric technology.

REFERENCES

[1] Phillips, P. J., Martin, A., Wilson, C. L., & Przybocki, M. (2000). An introduction evaluating biometric systems. Computer, 33(2), 56-63.

[2] Babich, A. (2012). Biometric Authentication. Types of biometric identifiers.

[3] Kong A, Zhang D, Kamel M, "A survey of palmprint recognition," Pattern Recognition, 2009, vol.42, pp.1408-1418, July, 2 009.doi:10.1016/j.patcog.2009.01.018.

[4] Wu Y P, Tian J W, Xu D, et al. "Palmprint Recognition Based on RB K-means and Hierarchical SVM", International Conference on Machine Learning & Cybernetics, 2007, doi:10.1109/ICMLC.2007.4370778.

[5] Zhang, D., Liu, L.L. (2009). Palmprint Features. In: Li, S.Z., Jain, A. (eds) Encyclopedia of Biometrics. Springer, Boston, MA.

[6] Ajay Kumar, David C. M. Wong, Helen C. Shen, Anil K. Jain, 2003, " Personal Verification Using Palmprint and Hand Geometry Biometric", Springer, Audio- and Video- Based Biometric Person Authentication Lecture Notes in Computer Science Volume 2688, pp668-678.

[7] A. Kumar and D. Zhang, "Integrating shape and texture for hand verification,"Third International Conference on Image and Graphics (ICIG'04)", 2004, pp. 222-225, doi: 10.1109/ICIG.2004.87.

[8] D. Zhang and W. Shu, "Two novel characteristics in palmprint verification: datum point invariance and line feature matching," Pattern Recognition, vol. 32, no. 4, pp. 691-702, Apr. 1999.

[9] M. M. H. Ali, P. Yannawar and A. T. Gaikwad, "Study Of Edge Detection Methods Based On Palmprint Lines," International Conference on Electrical, Electronics, and Optimization Techniques, 2016.

[10] P. Selvakumar and S. Hariganesh, "The performance analysis of edge detection algorithms for image processing", International Conference on Computing Technologies and Intelligent Data Engineering (ICCTIDE'16), 2016, pp. 1-5, doi: 10.1109/ICCTIDE.2016.7725371.

[11] K.N. Bharath, G. Padmajadevi, Kiran, "Hybrid Compression Using DWT-DCT and Huffman Encoding Techniques for Biomedical Image and Video Applications", International Journal of Computer Science and Mobile Computing, Vol. 2, Issue. 5, May 2013, pg.255 – 261.

[12] Daubechies I. Ten lectures on wavelets. Philadelphia: Society for Industrial and Applied Mathematics; 1992

[13] Mohammed AA, Hussein JA. Efficient hybrid transform scheme for medical image compression. Int J Comput Appl 2011;27:16–20.

[14] Paul Nii Tackie Ammah, Ebenezer Owusu, Robust medical image compression based on wavelet transform and vector quantization, Informatics in Medicine Unlocked 15, Elsevier, (2019) 100183.

[15] Figlu Mohanty, Suvendu Rup, Bodhisattva Dash, Banshidhar Majhi, M. N. S. Swamy, Digital mammogram classification using 2D-BDWT and GLCM features with FOA-based feature selection approach, Neural Computing and Applications, part of Springer Nature 2019, https://doi.org/10.1007/s00521-019-04186-w

[16] 12Keerthika C., Rajakumar K., "Medical Image Retrieval using Dual Tree Complex Wavelet Transform and Principal Component Analysis with Haralick Texture Features", International Journal of Recent Technology and Engineering (IJRTE) ISSN: 2277-3878, Volume-8 Issue-5, January 2020.

[17] Annarita Fanizzi, Teresa Maria Basile, Liliana Losurdo, Roberto Bellotti, Ubaldo Bottigli, Francesco Campobasso, Vittorio Didonna, Alfonso Fausto, Raffaella Massafra, Alberto Tagliafico, Pasquale Tamborra, Sabina Tangaro, Vito Lorusso and Daniele La Forgia, "Ensemble DiscreteWavelet Transform and Gray-Level Co-Occurrence Matrix for Microcalcification Cluster Classification in Digital Mammography", Applied Sciences 2019, 9, 5388; doi:10.3390/app9245388.

[18] Haralick, R.M.; Shanmugam, K.; Dinstein, I. Textural features for image classification. IEEE Trans. Syst. Man Cybern. 1973, 6, 610–621.

[19] Dipankar Hazra, "Texture Recognition with combined GLCM, "Wavelet and Rotated Wavelet Features", International Journal of Computer and Electrical Engineering, Vol.3, No.1, February, 2011, 1793-8163.

[20] Taner Çevik, Ali Mustafa Ali Alshaykha, Nazife Çevik, A Comprehensive Performance Analysis of GLCM-DWT-based Classification on Fingerprint Identification, International Journal of Computer Applications (0975 – 8887) Volume 180 – No.32, April 2018.

[21] Shankar Bhausaheb Nikam, Suneeta Agarwal, "Wavelet Energy Signature and GLCM Features-based fingerprint anti-spoofing", Proceedings of the 2008 International Conference on Wavelet Analysis and Pattern Recognition, Hong Kong, 30-31 Aug,2008.

[22] Manjunath B.S, Ma W.Y, "Texture features for browsing and retrieval of image data", IEEE Transactions on Pattern Analysis and Machine Intelligence, Vol. 18, No. 8, Aug,1996.

[23] Q Tian, N Sebe, M S Lew, E Loupias, T S Huang, " Image Retrieval using wavelet-based salient points", Journal of Electronic Imaging, Special Issue on Storage and Retrieval of Digital Media, pp.835-849, vol.10(4),Oct, 2001.

[24] Raghuveer M. Rao and Ajit S. Bopardikar, Wavelet Transforms: Introduction to Theory & Application, Pearson Education, India, 2009, pp. 66-73.

[25] M. Kakore, P.K. Biswas, B.N. Chatterjee, "Texture image retrieval using rotated wavelet filters", Pattern Recognition Letters 28, 1240-1249, 2007.

[26] K. Muneeswaran, L. Ganeshan, S.Arumugam and K. Ruba Soundar, "Texture classification with combined rotation and scale invariant wavelet features", Pattern Recognition 38,1495-1506, 2005.

[27] Tianhorng Chang and C C Jay Kuo, "Texture Analysis & Classification with Tree-

Structured Wavelet Transform", IEEE Transaction on Image Processing , vol-2, no 4, 1993.

[28] Alpana Jijja, Dinesh Rai, "Segmentation of Brain Tumor using Glcm and Discrete Wavelet Transform", International Journal of Innovative Technology and Exploring Engineering (IJITEE) ISSN: 2278-3075 (Online), Volume-9 Issue-6, April 2020.

[29] Ş. Öztürk and B. Akdemir, "Application of feature extraction and classification methods for histopathological image using GLCM, LBP, LBGLCM, GLRLM and SFTA", Procedia Computer Science, vol. 132, pp. 40-46, 2018

[30] Pathak, B.; Barooah, D. Texture analysis based on the gray-level co-occurrence matrix considering possible orientations. Int. J. Adv. Res. Electr. Electron. Instrum. Eng. 2013, 2, 4206–4212

[31] Mohanaiah, P.; Sathyanarayana, P.; GuruKumar, L. Image texture feature extraction using GLCM approach. Int. J. Sci. Res. Publ. 2013, 3, 1.

[32] Sujata,Rajesh Parihar, Vikas Sharma, "Detection and Classification of Tumor Type in Brain MRI images using SVM & Deep Learning Techniques", Wutan Huatan Jisuan Jishu , Volume XVI, Issue X, ISSN:1001-1749, OCT/2020.

[33] Alexander Selvikvåg Lundervolda & Arvid Lundervolda, "An overview of deep learning in medical imaging focusing on MRI", A.S. Lundervold, A. Lundervold / Z Med Phys 29 (2019)102–127.

[34] B.Gopinath, Dr.B.R.Gupta, "Majority Voting based Classification of ThyroidCarcinoma", Elsevier, Procedia Computer Science 2 (2010) 265–271.

[35] Dipankar Hazra," Texture Recognition with combined GLCM, Wavelet and Rotated Wavelet Features", International Journal of Computer and Electrical Engineering, Vol.3, No.1, February, 2011, 1793-8163.

[36] LI Yunfeng, ZHANG Yali, "Palmprint Recognition Based on Weighted Fusion of DMWT and LBP", 2011 4th International Congress on Image and Signal Processing, IEEE, 2011.

[37] Beura S, Majhi B, Dash R (2015) Mammogram classification using two dimensional discrete wavelet transform and gray-level co-occurrence matrix for detection of breast cancer. Neuro computing 154:1–14.

[38] Annarita Fanizzi, Teresa Maria Basile, Liliana Losurdo, Roberto Bellotti, Ubaldo Bottigli, Francesco Campobasso, Vittorio Didonna, Alfonso Fausto, Raffaella Massafra, Alberto Tagliafico, Pasquale Tamborra, Sabina Tangaro, Vito Lorusso and Daniele La Forgia, Ensemble DiscreteWavelet Transform and Gray-Level Co-Occurrence Matrix for Microcalcification Cluster Classification in Digital Mammography, Appl. Sci. 2019, 9, 5388; doi:10.3390/app9245388.

[39] Keerthika C., Rajakumar K., Medical Image Retrieval using Dual Tree Complex Wavelet Transform and Principal Component Analysis with Haralick Texture Features, International Journal of Recent Technology and Engineering (IJRTE) ISSN: 2277-3878, Volume-8 Issue-5, January 2020.

[40] Sujata,2Rajesh Parihar, 3Vikas Sharma, "Detection and Classification of Tumor Type in Brain MRI images using SVM & Deep Learning Techniques", Volume XVI, Issue X, OCT/2020.

[41] Alpana Jijja, Dinesh Rai, Segmentation of Brain Tumor using Glcm and Discrete Wavelet Transform, International Journal of Innovative Technology and Exploring Engineering (IJITEE) ISSN: 2278-3075, Volume-9 Issue-6, April 2020.

[42] Oliver Faust, Joel En Wei Koh, Vicnesh Jahmunah, Sukant Sabut, Edward J. Ciaccio, Arshad Majid, Ali Ali, Gregory Y. H. Lip and U. Rajendra Acharya, Fusion of Higher Order Spectra and Texture Extraction Methods for Automated Stroke Severity Classification with MRI Images, Int. J. Environmental. Research and Public Health 2021, 18, 8059. https://doi.org/10.3390/ijerph18158059.